USING e-ANNOTATION TOOLS FOR ELECTRONIC PROOF CORRECTION

Required software to e-Annotate PDFs: Adobe Acrobat Professional or Adobe Reader (version 8.0 or above). (Note that this document uses screenshots from Adobe Reader DC.)
The latest version of Acrobat Reader can be downloaded for free at: http://get.adobe.com/reader/

Once you have Acrobat Reader open on your computer, click on the Comment tab (right-hand panel or under the Tools menu).

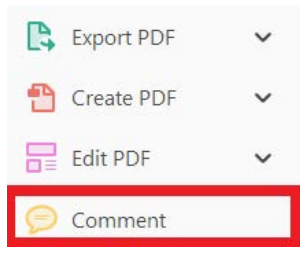

This will open up a ribbon panel at the top of the document. Using a tool will place a comment in the right-hand panel. The tools you will use for annotating your proof are shown below:

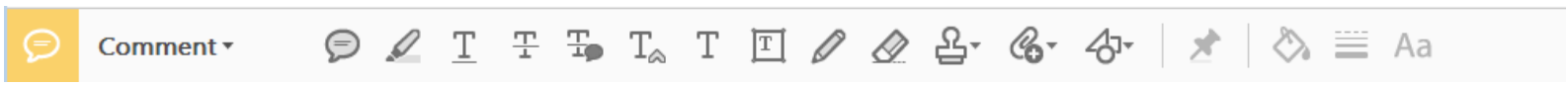

1. Replace (Ins) Tool – for replacing text.

Strikes a line through text and opens up a text box where replacement text can be entered.

How to use it:

- Highlight a word or sentence.
- Click on .
- Type the replacement text into the blue box that appears.

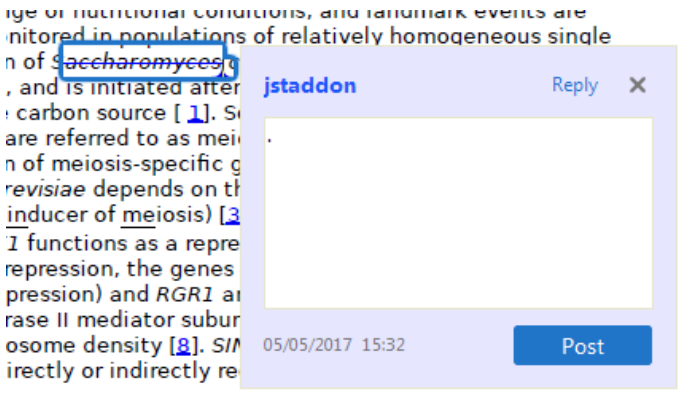

2. Strikethrough (Del) Tool – for deleting text.

Strikes a red line through text that is to be deleted.

How to use it:

- Highlight a word or sentence.
- Click on .
- The text will be struck out in red.

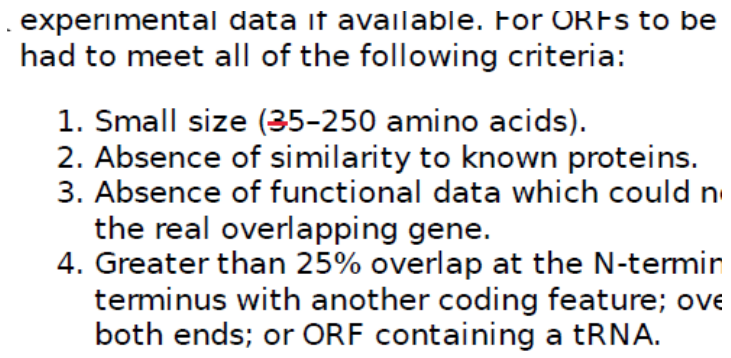

3. Commenting Tool – for highlighting a section to be changed to bold or italic or for general comments.

Use these 2 tools to highlight the text where a comment is then made.

How to use it:

- Click on .
- Click and drag over the text you need to highlight for the comment you will add.
- Click on .
- Click close to the text you just highlighted.
- Type any instructions regarding the text to be altered into the box that appears.

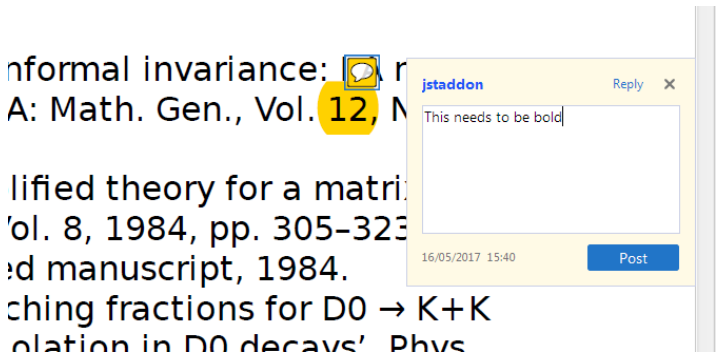

4. Insert Tool – for inserting missing text at specific points in the text.

Marks an insertion point in the text and opens up a text box where comments can be entered.

How to use it:

- Click on .
- Click at the point in the proof where the comment should be inserted.
- Type the comment into the box that appears.

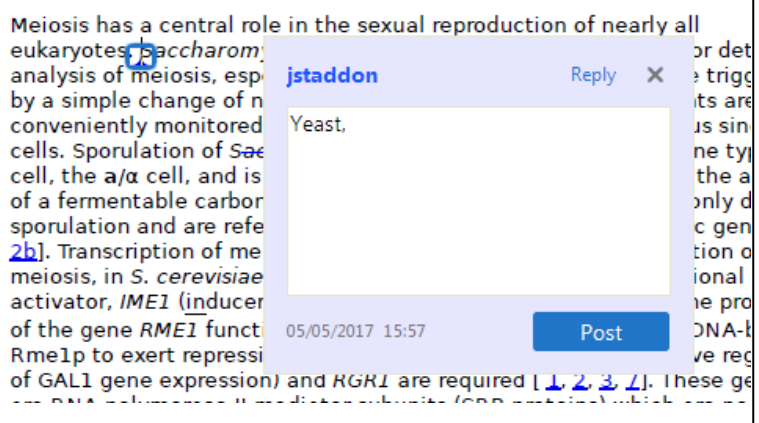

WILEY

USING e-ANNOTATION TOOLS FOR ELECTRONIC PROOF CORRECTION

5. Attach File Tool – for inserting large amounts of text or replacement figures.

Inserts an icon linking to the attached file in the appropriate place in the text.

How to use it:

- Click on  .
- Click on the proof to where you'd like the attached file to be linked.
- Select the file to be attached from your computer or network.
- Select the colour and type of icon that will appear in the proof. Click OK.

  The attachment appears in the right-hand panel.

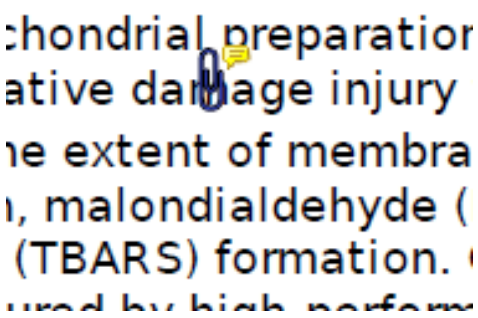

6. Add stamp Tool – for approving a proof if no corrections are required.

Inserts a selected stamp onto an appropriate place in the proof.

How to use it:

- Click on  .
- Select the stamp you want to use. (The Approved stamp is usually available directly in the menu that appears. Others are shown under *Dynamic*, *Sign Here*, *Standard Business*).
- Fill in any details and then click on the proof where you'd like the stamp to appear. (Where a proof is to be approved as it is, this would normally be on the first page).

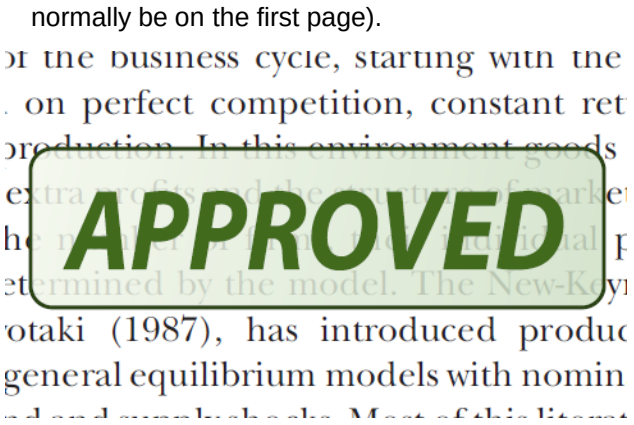

Drawing tools available on comment ribbon

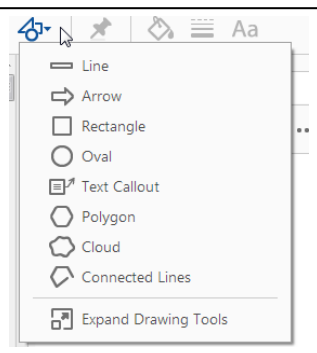

7. Drawing Markups Tools – for drawing shapes, lines, and freeform annotations on proofs and commenting on these marks.

Allows shapes, lines, and freeform annotations to be drawn on proofs and for comments to be made on these marks.

How to use it:

- Click on one of the shapes in the Drawing Markups section.
- Click on the proof at the relevant point and draw the selected shape with the cursor.
- To add a comment to the drawn shape, right-click on shape and select *Open Pop-up Note.*
- Type any text in the red box that appears.

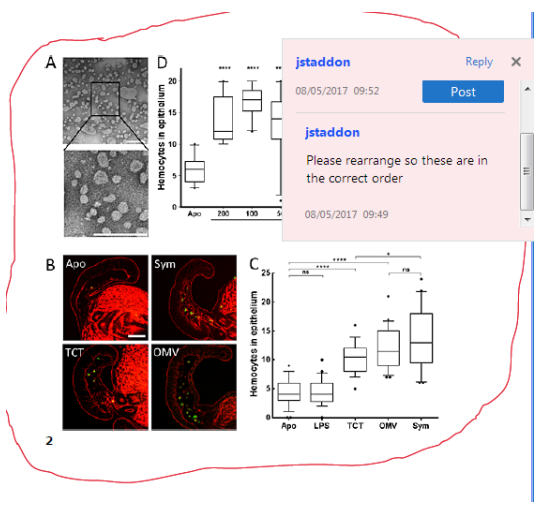

For further information on how to annotate proofs, click on the Help menu to reveal a list of further options:

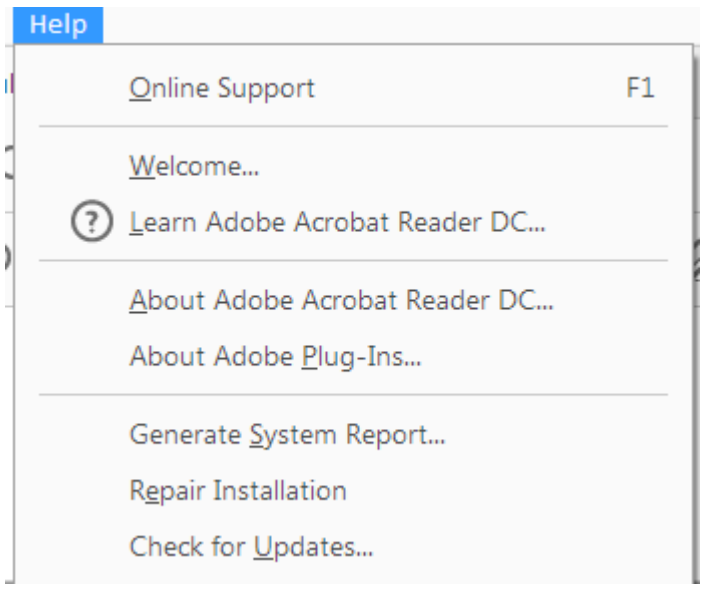

physica status solidi a
www.pss-a.com
applications and materials science

WILEY-VCH

Dear Author,

Please correct your galley proofs carefully and return them no more than four days after the page proofs have been received.

The editors reserve the right to publish your article without your corrections if the proofs do not arrive in time.

Note that the author is liable for damages arising from incorrect statements, including misprints.

Please note any queries that require your attention. These are indicated with a Q in the PDF and a question at the end of the document.

Please limit corrections to errors already in the text; cost incurred for any further changes or additions will be charged to the author, unless such changes have been agreed upon by the editor.

Reprints may be ordered by filling out the accompanying form.

Return the reprint order form by fax or by e-mail with the corrected proofs, to Wiley-VCH : **pssa.corr@wiley-vch.de**

To avoid commonly occurring errors, please ensure that the following important items are correct in your proofs (please note that once your article is published online, no further corrections can be made):

- **Names** of all authors present and spelled correctly
- **Titles** of authors correct (Prof. or Dr. only: please note, Prof. Dr. is not used in the journals)
- **Addresses** and **postcodes** correct
- **E-mail address** of corresponding author correct (current email address)
- **Funding bodies** included and grant numbers accurate
- **Title** of article OK
- All **figures** included
- **Equations** correct (symbols and sub/superscripts)

Corrections should be made directly in the PDF file using the PDF annotation tools. If you have questions about this, please contact the editorial office. The corrected PDF and any accompanying files should be uploaded to the journal's Editorial Manager site.

physica status solidi a

www.pss-a.com

applications and materials science

Editorial Office:

Wiley-VCH Verlag, Rotherstrasse 21
10245 Berlin, Germany

Tel.: +49(0)30-47031-331
Fax: +49(0)30-47031399

E-mail: pssa.corr@wiley-vch.de
www.pss-journals.com

Reprint Order Form 2017
- please return with your proofs -

Manuscript No. _____

Please send me and bill me for

☐ no. of **reprints** via ☐ airmail (+ 25 Euro) ☐ surface mail

☐ no. of **copies of this issue** (1 copy: 25 Euro) via ☐ airmail (+ 25 Euro) ☐ surface mail

☐ **high-resolution PDF file** (330 Euro).
My e-mail address:

_____

Please note: It is not permitted to present the PDF file on the internet or on company homepages

★**Special Offer**★ If you order 200 or more reprints you will get a PDF file for half price.

Information regarding VAT
Please note that from German sales tax point of view, the charge for **Reprints, Issues or Posters** is considered as **"supply of goods"** and therefore, in general, such delivery is a subject to German sales tax. However, this regulation has no impact on customers located outside of the European Union. Deliveries to customers outside the Community are automatically tax-exempt. Deliveries within the Community to institutional customers outside of Germany are exempted from the German tax (VAT) only if the customer provides the supplier with his/her VAT number. The VAT number (value added tax identification number) is a tax registration number used in the countries of the European Union to identify corporate entities doing business there. It starts with a country code (e.g. FR for France, GB for Great Britain) and follows by numbers.

Cover Posters

Posters are available of all the published covers and frontispieces in two sizes

☐ DIN A2 42 x 60 cm / 17 x 24in (one copy: **39 Euro**)
☐ DIN A1 60 x 84 cm / 24 x 33in (one copy: **49 Euro**)

Postage for shipping posters overseas by airmail:
+ 25 Euro
Postage for shipping posters within Europe by surface mail:
+ 15 Euro

Mail reprints /cover posters / copies of the issue to:

_____
_____
_____
_____
_____

Invoice address:

_____
_____
_____
_____
_____

_____
Date, Signature **Stamp**

VAT no.: _____
(institutes / companies in EU countries only)

Purchase Order No.: _____

Credit Card Payment

VISA, MasterCard, AMERICAN EXPRESS
Please use the Credit Card Token Generator located at the website below to create a token for secure payment. The token will be used instead of your credit card number.

Credit Card Token Generator:
https://www.wiley-vch.de/editorial_production/index.php

Please transfer your token number to the space below.

Credit Card Token Number:

Price list for reprints (The prices include mailing and handling charges. All Wiley-VCH prices are exclusive of VAT)

No. of pages	Price (in Euro) for orders of 50 copies	100 copies	150 copies	200 copies	300 copies	500 copies
1-4	345	395	425	445	548	752
5-8	490	573	608	636	784	1077
9-12	640	739	786	824	1016	1396
13-16	780	900	958	1004	1237	1701
17-20	930	1070	1138	1196	1489	2022
for every additional 4 pages	147	169	175	188	231	315

★ **Special Offer** ★ If you order 200 or more reprints you will get a PDF file for half price.

Wiley-VCH Verlag GmbH & Co. KGaA; Location of the Company: Weinheim;
Chairman of the Supervisory Board: Stephen Michael Smith,
Trade Register: Mannheim, HRB 432833, General Partner: John Wiley & Sons GmbH,
Location: Weinheim, Trade Register Mannheim, HRB 432296,
Managing Director: Sabine Steinbach

WILEY-VCH

WILEY

AUTHOR QUERY FORM

JOURNAL: PHYSICA STATUS SOLIDI (A)

Article: pssa201800275

Dear Author,

During the copyediting of your manuscript the following queries arose.

Please refer to the query reference callout numbers in the page proofs and respond to each by marking the necessary comments using the PDF annotation tools.

Please remember illegible or unclear comments and corrections may delay publication.

Many thanks for your assistance.

Query No.	Query	Remark
Q1	Please confirm that given names (blue) and surnames/family names (vermilion) have been identified correctly.	
Q2	Please check all equations have been correctly typeset.	
Q3	Please check the presentation of Acknowledgements section for correctness.	
Q4	We have inserted the conflict of interest statement below acknowledgements section. Please check and approve.	

Please confirm that the funding sponsor list below was correctly extracted from your article: that it includes all funders and that the text has been matched to the correct FundRef Registry organization names. If a name was not found in the FundRef registry, it may not be the canonical name form, it may be a program name rather than an organization name, or it may be an organization not yet included in FundRef Registry. If you know of another name form or a parent organization name for a "not found" item on this list below, please share that information.

FundRef name	FundRef OrganizationName (Country)
	MINECO/FEDER/M-ERA.Net. Cofund
	PAPIIT-UNAM

physica status solidi a
www.pss-a.com

Surface Dielectric Tunnel Barrier Induced by Mn Doping in SnO_2 Micro- and Nanostructures

Manuel Herrera, David Maestre,* and Ana Cremades

Electrical properties of undoped and Mn doped SnO_2 microplates and rods have been studied by electron beam induced current (EBIC) in a scanning electron microscope (SEM), and I–V curves acquired at room temperature. AFM measurements reveal the formation of numerous terraces at the (−101) surface of the analyzed Mn-doped SnO_2 microplates, which also exhibit high carrier recombination processes at their central region, as confirmed by combined EBIC and cathodoluminescence (CL) measurements. A diffusion length for minority carriers about 205 nm is obtained by EBIC measurements. Different electrical conduction mechanisms, such as Fowler-Nordheim, Direct Tunneling and Poole-Frenkel, have been evaluated in the electrical analysis of the samples. Mn doped microplates show lower conductivity than the undoped microds. Moreover the height of the surface tunnel barrier is increased by Mn doping, as confirmed by the analysis of the I–V curves acquired under transversal configuration. A value of the relative dielectric constant ε_r about 7.3 has been estimated for the probed SnO_2 microstructures.

1. Introduction

SnO_2 is a semiconductor with a direct wide bandgap of about 3.6 eV (at 300 K) that receives significant attention due to their applications as gas sensors, solar cells, or catalyst.[1–4] Moreover, SnO_2-based elongated micro- and nanostructures can be also used as building blocks in optoelectronic devices. The combination of good electrical conductivity, due to the intrinsic oxygen deficiency, together with high transparency in the visible range makes this material one of the most exploited transparent conductive oxides (TCO). Moreover, Mn doping can induce variations in the SnO_2 electrical and optical properties, together with magnetic functionality, what motivates its study. This semiconductor has also been proposed for spintronic applications due to the ferromagnetic properties observed at room temperature, particularly in Mn-doped SnO_2 thin films and nanostructures.[5–8] The use of spin-MOSFET's with gate electrodes composed by a ferromagnetic material with the insertion of a dielectric barrier at the gate, enhances the spin accumulation at the semiconductor at room temperature due to the increase of interface resistance by the formation of a tunnel barrier.[9,10] On the other hand, tunnel barriers produced as dielectric layers in semiconductors, or dielectric tunnel barriers, demonstrate direct applications in the fabrication of information storage devices,[11] such as floating gate field-effect transistors used in cellular phones, and digital cameras. These barriers are fabricated and investigated mainly from materials with high dielectric constant, such as Al_2O_3, SiO_2, Ta_2O_5, HfO_2 and $ZrSi_xO_y$,[12] and less have been done on the potential candidate SnO_2 so far. In some of these applications, the mechanisms involved in the electronic conduction strongly influence the final device performance, hence a deep study of these processes is required.

Previously, we reported that the presence of Mn induced changes in the growth conditions and the morphology of Mn-doped SnO_2 micro- and nanostructures grown by a vapor–solid method, as well as in their luminescence.[13] Temperatures, around 1090 °C, are required to synthesize Mn doped SnO_2 microplates, with lengths of tens of microns, thickness below 1 μm and widths between 2 and 4 μm. Following this synthesis method, wires and belts could be fabricated as well. Electron backscattered diffraction measurements indicate that the microplates grow along the [101] direction. We also reported that the average of Mn content incorporated in the SnO_2 is around 1.6 at %, as measured by EDS, although the incorporation of Mn varies as a function of the probed surface of the microplate, as confirmed by XPS measurements.[13] Facets with a higher amount of Mn are associated with increased luminescence due to a higher concentration of oxygen vacancies related defects, as the presence of Mn^{3+} substituting Sn^{4+} involves formation of oxygen vacancies to maintain charge neutrality. In this case, as a further investigation, we study the effects caused by Mn doping on the electrical properties of these SnO_2 micro- and nanostructures grown by a vapor–solid process. We report that the electrical conduction mechanism, at room temperature, in Mn

Dr. M. Herrera, Dr. D. Maestre, Prof. A. Cremades
Departamento de Física de Materiales
Universidad Complutense de Madrid
Madrid 28040, Spain
E-mail: dmaestre@ucm.es
Dr. M. Herrera
Centro de Nanociencias y Nanotecnología
Universidad Nacional Autónoma de México
22800-Ensenada, Baja California, México

Dedicated to Prof. Javier Piqueras

DOI: 10.1002/pssa.201800275

doped SnO_2 elongated structures reveals the formation of a dielectric tunnel barrier at their surface. The influence of Mn doping in the formation of this tunnel barrier is discussed in this work.

2. Experimental Section

The undoped and Mn doped SnO_2 microstructures analyzed in this work were grown by a catalyst-free evaporation-deposition method, following a procedure that we previously reported in Ref. [13]. In order to synthesize Mn doped SnO_2 samples, commercial powders of SnO_2 (Alfa Aesar 99.99%) and $MnCO_3$ (Alfa Aesar 99.9%) at 5 wt% were mechanically mixed in a centrifugal ball mill and thermally treated under a controlled Ar flow in a horizontal furnace operated at 1400 °C for 10 h under low vacuum conditions (up to 1×10^{-2} mbar). A SnO_2 ceramic substrate, previously sintered at 700 °C, was placed at the downstream side of the furnace, where different elongated nano- and microstructures grow by a vapor–solid process as a function of the temperature.[13] In particular, Mn doped SnO_2 microplates are grown at 1090 °C. A reference sample of undoped SnO_2 microrods and wires, grown at 1040 °C, was also prepared by the same method using pure SnO_2 as precursor.

The morphology of these micro- and nanostructures was studied with a Leica 440 Stereoscan SEM operated at 10 kV and 500 pA. Atomic Force Microscopy (AFM) measurements were performed at atmospheric pressure, using a Nanotech AFM controlled by a Dulcinea software operated in contact mode with commercial Si tips. For AFM observations, some of the structures under study were placed onto a Si (100) substrate and fixed with silver paint. The electrical properties of the as-grown structures were studied by Electron Beam Induced Current (EBIC) in a scanning electron microscope (SEM) at room temperature and low vacuum conditions ($\approx 10^{-6}$ Torr). Considering tin oxide as a n-type semiconductor, as commonly reported, and work function values of about 4.5, 4.1, and 4.8 eV for SnO_2, In and Au, respectively, either Schottky or ohmic contacts will be obtained by Au/SnO_2 or In/SnO_2. For EBIC measurements the Mn doped SnO_2 microplates were deposited onto a Au/Si(100) substrate generating a SnO_2/Au Schottky contact in planar configuration. The second electrode consists of an electrochemically etched W tip coated with In attached to a micromanipulator in a Leica 440 SEM, used to contact the surface of the SnO_2 microplates as an ohmic contact (In/SnO_2) in order to perform EBIC measurements. Local I–V measurements have been also acquired under transversal configurations in an SEM at room temperature and low vacuum conditions ($\approx 10^{-6}$ Torr), using a Keithley 2400 as power supply and amperemeter. The structures were placed onto a In/Si(100) substrate, in order to obtain a SnO_2/In ohmic contact, while the micro-manipulated In/W tip was used as the second electrode, therefore the current flows through the structure.

3. Results and Discussion

SEM image in **Figure 1**a shows a Mn-doped SnO_2 microplate with a length and width of about 30 and 5 μm, respectively, which was placed onto a Si(100) substrate and fixed with silver paint to be studied by AFM. Figure 1b shows an AFM image of the region marked with a square in Figure 1a. The AFM study reveals a surface formed by parallel terraces aligned along the growth direction of the microplate, marked with an arrow in Figure 1b, which has been previously identified as the [10-1].[13] These terraces, the concentration of which is higher in the central region of the microplates, show the same triangular-ending appearance observed in the microplates. The topographic profile shown in Figure 1c corresponds to the line marked in the terrace in Figure 1b, which indicates that terraces at the surface of the microplate present a step-height of about 15 Å. EBSD study of the Mn doped SnO_2 microplates revealed that their main surface corresponds to the rutile (−101) plane.[13] Considering that the thickness of an atomic monolayer of the (−101) surface in SnO_2 is 5.2 Å, the terrace profiled in Figure 1c could roughly correspond to three atomic monolayers. The correlative EBDS-CL-XPS study referred in Ref. [13] enabled us to associate the (−101) surface with a region of hindered Mn incorporation, low presence of oxygen vacancies, and high concentration of surface defects.

In this work, EBIC measurements in a SEM have been carried out on the Mn doped SnO_2 microplates in order to analyze their electrical behavior. **Figure 2**a,b show SEM and EBIC images, respectively, of a Mn doped SnO_2 microplate placed onto a Au-coated Si substrate and electrically connected with an indium-coated W tip. A significant dark contrast along the central region of the microplate is clearly observed in the EBIC image (Figure 2b). Dark contrast in EBIC images corresponds to low electric currents collected by the In/W tip electrode, which can be attributed to a decrease of the charge carrier density due to recombination of electron-hole pairs.[14] Extended defects, such as dislocations and grain boundaries, typically result in dark EBIC contrasts, as they usually act as radiative recombination centers.[15–17] In this case, the presence of radiative recombination centers at the central region of the Mn doped SnO_2 microplates has been confirmed by CL measurements, as shown in Figure 2c where the central region of the microplates appear brighter. In particular the CL signal associated with the microplates is dominated by a blue emission of 2.58 eV,[13] usually attributed to shallow levels in the SnO_2 electronic structure involving surface defects, removal of oxygen vacancies, and/or creation of oxygen interstitials.[18] Therefore a higher concentration of these defects should be present in the central region of the microplates, showing a brighter CL signal, where AFM measurements also indicate a higher presence of terraces. Figure 2d shows an EBIC profile corresponding to the line marked in the EBIC image (inset), which corresponds to the central region of the microplate in Figure 2b. By neglecting surface recombination, EBIC signal decays exponentially following the expression $I \propto \exp(-x/L)$, where I is the EBIC signal, x is the length from the bright region with high e-h recombination, and L corresponds to the diffusion length of the minority carriers. In this case, L was estimated using the fit of Figure 2d, obtaining a value of (205 ± 18) nm, in agreement with values reported for SnO_2 ceramic material between 0.2 and 2 μm.[19]

I–V measurements have been performed on the Mn doped SnO_2 micro and nanostructures, as well as on undoped SnO_2 low dimensional structures, as a reference, by using ohmic contacts

COLOR

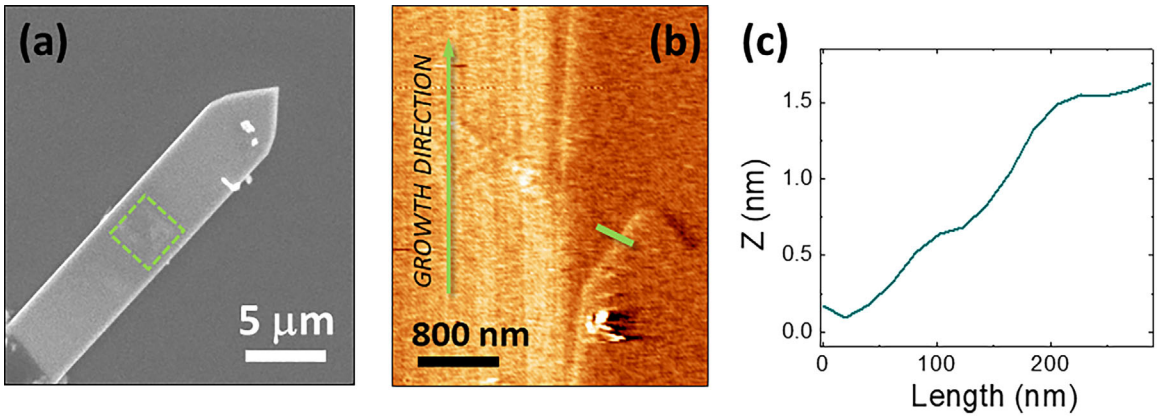

Figure 1. a) SEM image of a Mn doped SnO_2 microplate. b) AFM image obtained from the square marked in (a). c) AFM profile measured along the line marked in the terrace in (b).

under transversal configuration at low vacuum conditions in a SEM. Different structures have been analyzed in this work, so that the results here shown can be considered as representative for the samples under study. In addition, different conduction mechanisms have been considered in the analysis of the I–V curves, such as ohmic conduction, Fowler-Nordheim tunneling (FN), Direct Tunneling (DT), Poole-Frenkel (PF), Schottky emission, or Space-Charge-Limited conduction (SCL). As the I–V curves have been acquired in a SEM at room temperature, temperature-related effects have not been considered in the electrical analysis. Moreover, additional I–V curves have been acquired as a reference contacting directly the In/W tip and the In/Si substrate, without any SnO_2 structure in between. As the corresponding I–V curves exhibit an ohmic behavior, we disregard the presence of a possible dielectric layer at the In/W tips or the In/Si substrate that could act as a potential barrier, which will be further taken into account in the analysis of the I–V curves.

Firstly, Mn doped SnO_2 microplates with an amount of Mn about 1.6 at%, as those shown in Figure 1a, have been electrically characterized. **Figure 3**a shows the I–V curve corresponding to a microplate, with a thickness about 500 nm, electrically connected between the In/Si substrate and the In/W tip, as observed in the SEM image shown in the inset. Two bias regimes, below and over 20 V, can be clearly appreciated in the corresponding non-linear I–V curve shown in Figure 3a, which suggests different conduction mechanisms involved for low or high bias voltage. A continuous increase of the current intensity up to

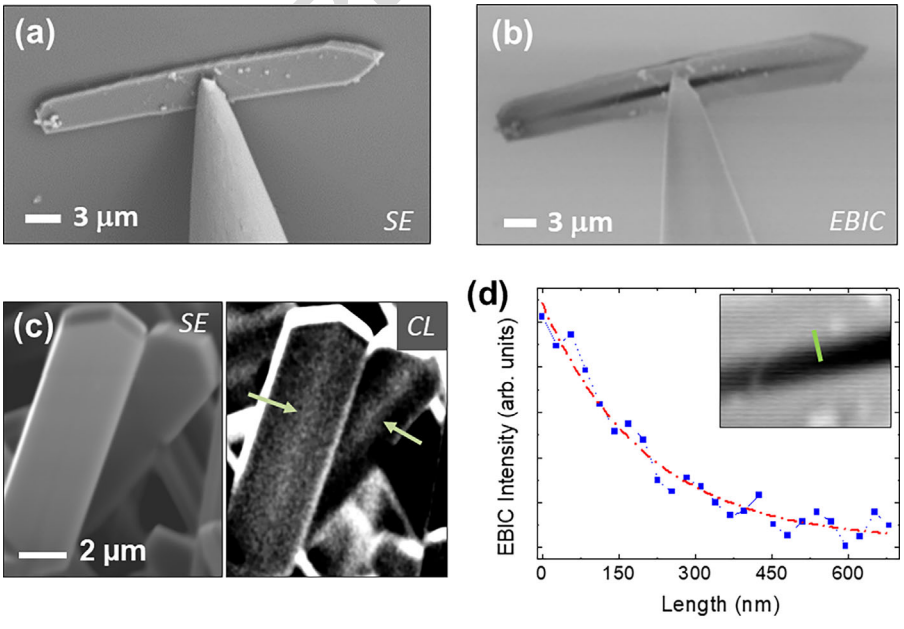

COLOR

Figure 2. a) SEM and (b) EBIC images of a Mn doped SnO_2 microplate. c) SEM and CL images acquired from Mn doped SnO_2 microplates. d) EBIC profile measured at the contrasted EBIC region shown in the inset.

COLOR

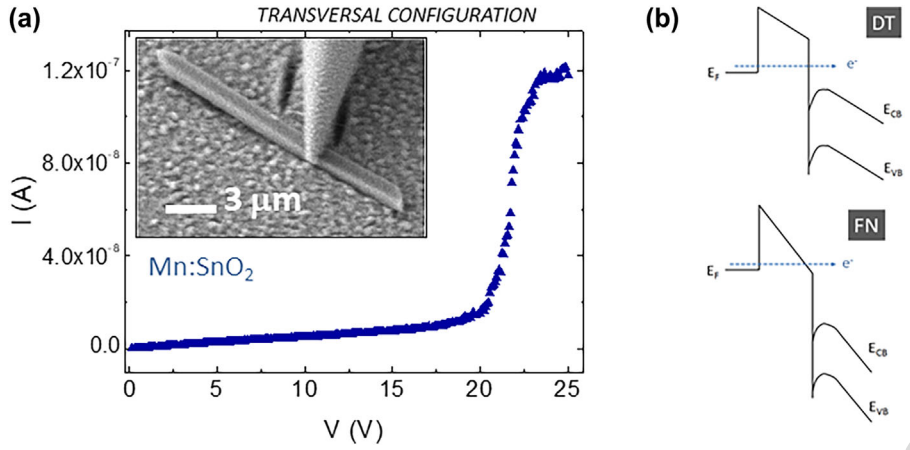

Figure 3. a) I–V curve acquired from a Mn doped SnO_2 microplate in transversal configuration. The inset shows the SEM image acquired before the measurement. b) Schematic descriptions of the direct-tunneling (DT) and Fowler-Nordheim (FN) conduction mechanisms.

several nA is observed when the applied voltage ranges between 0 and 20 V, while a strong increase of the current intensity up to 10^{-7} A is observed when the bias voltage is higher than 20 V, in accordance to the variation in the specific barrier profile.

Among the conduction mechanisms considered in this study, FN and DT can be fitted to the experimental I–V data in Figure 3a. FN involves electrons tunneling through a triangular potential barrier in the presence of a high electric field, while DT occurs when electrons are able to tunnel through a trapezoidal barrier not severely deformed at low electric fields (as shown in the schemes in Figure 3b). The high voltage regime (higher than 20 V) in Figure 3a, can be interpreted on the basis of the Fowler-Nordheim (FN) tunneling mechanism described by the relation[20]:

$$I(V) = \frac{A_{\text{eff}} \cdot q^3 \text{mV}^2}{8\pi h \phi_B d^2 m*} \exp\left(\frac{-8\pi\sqrt{2m*}\phi_B^{3/2} d}{3hqV}\right) \quad (1)$$

where A_{eff} is the effective contact area, ϕ_B is the barrier height, and q, m^*, d, and h correspond to the electron charge, effective electron mass for SnO_2, the separation between electrodes (microplate thickness), and the Planck's constant, respectively.

This equation can be rewritten as:

$$In\left(\frac{I}{V^2}\right) = In\left(\frac{A_{\text{eff}} \cdot q^3 m}{8\pi h \phi_B d^2 m*}\right) - \frac{8\pi\sqrt{2m*}}{3hqV}\phi_B^{3/2} d \quad (2)$$

Therefore, the FN mechanism in the high bias regime can be determined by a negative slope when plotting $ln(I/V^2)$ versus $(1/V)$, as shown in **Figure 4**a. Considering an effective mass for electrons in SnO_2 of $m^* = 0.27 m_0$,[21] a value of barrier height about $\phi_B = (0.42 \pm 0.08)$ eV can be obtained from the linear fit (Eq. 2) shown in Figure 4a. This result demonstrates that the FN tunneling originates the increase of the current intensity at high bias regime.

For the electrical conduction at low bias voltages between 0 and 20 V, a Direct-Tunneling (DT) mechanism has been considered. This mechanism, for which tunneling of electric charge occurs through a potential barrier, can be described by the following equation[22]:

$$I(V) = \frac{A_{\text{eff}} \cdot \sqrt{m\phi_B q^2 V}}{h^2 d} .\exp\left(\frac{-4\pi\sqrt{m\phi_B d}}{h}\right) \quad (3)$$

where m is the free electron mass, ϕ_B corresponds to the height of the potential barrier, and d is the width of the tunnel barrier. Usually this equation is rewritten as:

$$ln\left(\frac{I}{V^2}\right) = ln\left(\frac{A_{\text{eff}} \cdot \sqrt{m\phi_B q^2}}{h^2 d}\right) - \frac{4\pi\sqrt{m\phi_B d}}{h} + ln\left(\frac{1}{V}\right) \quad (4)$$

In this case, a DT mechanism can be identified as a linear fit in a plot of $ln(I/V^2)$ versus $ln(1/V)$, as shown in Figure 4b, where the slope should be ideally 1. The accurate linear fit, indicated in Figure 4b, leads to a slope of (1.02 ± 0.01) with an R^2 coefficient of 0.998, thus confirming the linear dependence expressed in Equation (4). However, despite the fact that the experimental data can be linearly fitted yielding a remarkably low value for the barrier height of $\phi_B = (0.7 \pm 0.2)\ 10^{-3}$ eV, electron tunneling through a potential barrier with a width of 500 nm, the thickness of the microplate, results physically improbable. Therefore, as some other conduction mechanisms have been considered and discarded in the analysis of the low bias regime, a modified direct tunneling mechanism is proposed in this work. In this case, the transversal configuration on which the I–V curves have been acquired, can be modeled as two tunnel barriers (In/SnO_2 and SnO_2/In), together with a current flow through the SnO_2 microplate. Following this idea, the total bias voltage can be interpreted as $V_{DT1} + V_{SnO_2} + V_{DT2}$. The origin of the both tunnel barriers could be related to the presence of surface states which can promote formation of depletion layers at the SnO_2 surface. If we assume that both In/SnO_2 and SnO_2/In barriers exhibit a similar behavior, as both corresponds to the (−101) planes, the total voltage, V, can be interpreted as $2V_{DT} + V_{SnO_2}$. Therefore, Equation (3) can be rewritten as:

COLOR

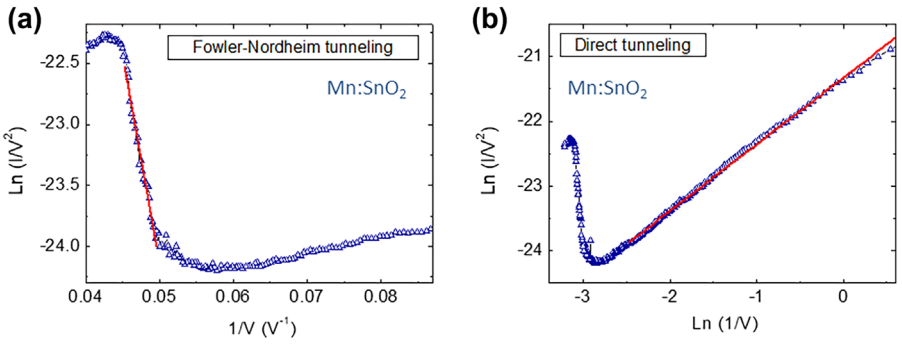

Figure 4. Fitting of the I–V curve in **Figure 3**a by using the models for (a) Fowler-Nordheim and (b) direct tunneling conduction mechanisms.

$$I(V) = \frac{A}{2e^{-B} + \mathrm{AR}_{\mathrm{SnO_2}}} V \tag{5}$$

with $= \frac{A_{\mathrm{eff}} \cdot \sqrt{m\phi_B q^2}}{h^2 d}$, $B = \frac{-4\pi\sqrt{m\phi_B d}}{h}$, and $R_{\mathrm{SnO_2}}$ is the electric resistance of the SnO_2.

In this case, d corresponds to the thickness of each tunnel barrier formed at the surface of the Mn doped SnO_2 microplate, in both contact regions, which in this work has been considered as around 5 nm, by following the values reported in some other works.[23,24] For $R_{\mathrm{SnO_2}}$ a value of 200 M Ω^{-1} has been considered, as estimated from the I to V curves shown in this work.

Therefore, Equation (5) can be expressed as:

$$ln\left(\frac{I}{V^2}\right) = ln\left(\frac{A}{2e^{-B} + \mathrm{AR}_{\mathrm{SnO_2}}}\right) + ln\left(\frac{1}{V}\right) \tag{6}$$

We found that the plot $ln(I/V^2)$ versus $ln(1/V)$ should also reveal a slope near to the unity. In this case, a value of (1.02 ± 0.01) was estimated for the slope in Figure 4b, enabling us to determinate the value for the barrier height of $\phi_B = (1.34 \pm 0.24)$ eV, which is more physically probable than the value of ϕ_B obtained before, even when this model can be further optimized.

Undoped SnO_2 rods have also been electrically analyzed in a SEM under transversal configuration for comparison. A microrod (250 nm thick) has been placed onto a In/Si substrate and pinned with an In/W electrode to assure a good electrical contact, as shown in the inset of **Figure 5**a. As a first difference with respect to the Mn doped SnO_2 structures (Figure 3a), the I–V curves from undoped SnO_2 do not show two clear bias regimes. Moreover, current values obtained for undoped SnO_2 are some orders of magnitude higher than those corresponding to Mn doped SnO_2 acquired using a similar transversal configuration. Actually, current values about 500 nA were achieved for undoped SnO_2 microrods with a bias voltage of 1 V, as shown Figure 5a, while for Mn-doped SnO_2 microplates similar values of current were not reached even with applied bias voltages of 25 V (Figure 3a). Even when differences in the thickness of the probed structures are considered in the electrical analysis, these results indicate that undoped SnO_2 microrods show higher conductivity than the Mn-doped SnO_2 microplates. FN and DT mechanisms have been also evaluated in comparison with the analysis of the I–V curves from Mn-doped SnO_2. In this case FN tunneling is not the dominant conduction mechanism, as data corresponding to the higher bias values cannot be linearly fitted when plotting $ln(I/V^2)$ versus $1/V$. On the other hand, Figure 5b shows the linear dependence when plotting $ln(I/V^2)$ versus $ln(1/V)$ for low voltages, with a slope of (0.97 ± 0.01), near to the theoretical value of 1 corresponding to DT. As conventional direct tunneling through a barrier of 250 nm, the thickness of the rod, is physically improbable, again a modified direct tunneling (Eq. 5) has been used to analyze the I–V curves, and a potential barrier of $\phi_B = (0.96 \pm 0.18)$ eV has been estimated in this case. This value is about 30% lower than the corresponding for Mn-doped SnO_2, obtained with a similar electrical analysis, which indicates that Mn doping induces an increase in the barrier height. This higher barrier height formed at the surface of the Mn-doped SnO_2

COLOR

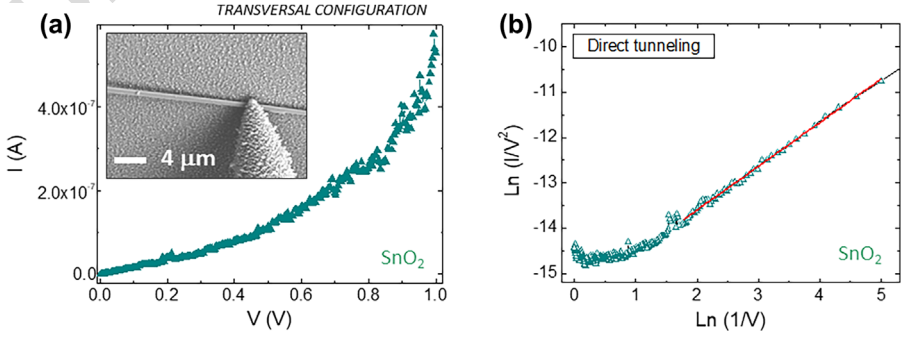

Figure 5. a) I–V curve acquired from an undoped SnO_2 microrod in transversal configuration. The inset in (a) shows the SEM image acquired before the measurement. b) Fitting of the I–V curve in (a) with the direct tunneling model.

microplates can be also associated with the increase in the resistivity of the Mn doped samples, as compared with undoped SnO_2.

As the presence of a dielectric layer acting as a potential barrier at the In/W tip or the In/Sn substrate was previously discarded, the electrical behavior deduced from the analysis of the I–V curves, could indicate that a dielectric tunnel barrier is formed at the probed (−101) surface of the Mn doped SnO_2 microplates. This barrier could be associated with a depletion layer formed due to surface states on SnO_2 (−101), which concentration would be increased for the Mn doped SnO_2 samples. Actually, previous cathodoluminescence measurements revealed a lower concentration of oxygen vacancies (V_O) in the Mn doped SnO_2 microplates,[13] mainly at the (−101) surface. This could explain the associated decrease in the conductivity induced by Mn doping, as these V_O defects govern the conductivity in SnO_2.[25,26]

In this work, a Poole-Frenkel (PF) mechanism, generated by a field-enhancement thermal excitation of trapped electrons into the conduction band, has been also considered in the analysis of the I–V curves. A scheme describing this trap-assisted conduction mechanism is depicted as an inset in **Figure 6a**. This mechanism follows the relation[27]:

$$I = \frac{qN_c\mu V}{d}\exp\left(\frac{\beta_{PF}V^{1/2} - q\phi_{PF}}{k_BT}\right) \quad (7)$$

where ϕ_{PF} is the Poole-Frenkel barrier height, k_B the Boltzmann constant, and β_{PF} is a coefficient related to the relative static permittivity, or dielectric constant ε_r, of the material by:

$$\beta_{PF} = \sqrt{\frac{e^3}{d\pi\varepsilon_0\varepsilon_r}} \quad (8)$$

where ε_0 is the vacuum permittivity, ε_r is the dielectric constant of SnO_2, e the electron charge and d corresponds to the nanostructure length between contacts. Equation (7) can be expressed as:

$$ln\left(\frac{I}{V}\right) = \frac{\beta_{PF}V^{1/2}}{k_BT} - \frac{q\phi_{PF}}{k_BT} + ln\frac{qN_c\mu}{d} \quad (9)$$

A value of $T = 300$ K has been considered in this analysis, although higher values could be locally achieved, as high bias voltages were used. According to Equation (9), PF mechanism implies a linear dependence of $ln(I/V)$ versus $V^{1/2}$, with slope values usually ranging from 1 to 2. In the case of Mn-doped SnO_2 microplates, I–V data cannot be fitted to Equation (9), indicating that PF is not the dominant conduction mechanism in this case. On the other hand, a good correlation has been found for undoped SnO_2 microrods (Figure 6a) in the region with voltages higher than 0.5 V in Figure 5a, which suggests that the PF mechanism is involved for high voltage values, complementary to the direct tunneling observed for low bias. Figure 6a shows the corresponding $ln(I/V)$ versus $V^{1/2}$ curve, from which analysis a value of 7.3 has been estimated for the dielectric constant ε_r. Reports on the permittivity values of SnO_2 nanostructures are scarce, and usually depend on the presence of dopants and concentration of oxygen vacancies.[28] Nevertheless, values for ε_r between 2.5 and 9.5 have been reported for SnO_2,[3,29] which agrees with the value obtained in this work.

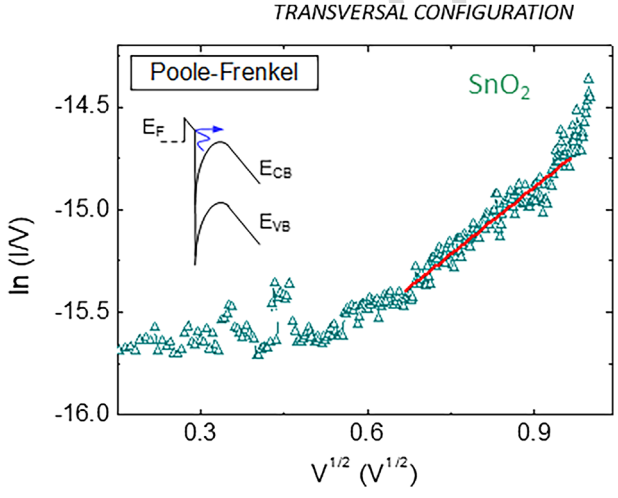

Figure 6. Fitting of the I–V curve shown in **Figure 5**a to the Poole-Frenkel conduction mechanism. A scheme of the PF model is included as an inset.

4. Conclusion

To summarize, in this work the electrical properties of undoped and Mn doped SnO_2 microplates and rods have been analyzed by EBIC technique and I–V curves acquired in transversal configuration. Topographic characterization by AFM shows formation of terraces at the (−101) surface of the Mn doped SnO_2 microplates. Combined EBIC and CL imaging techniques, reveal enhancement of carrier recombination along the central region of the Mn-doped SnO_2 microplates. Based on the analysis of the EBIC measurements, a value about 205 nm has been estimated for the diffusion length of the minority carriers. Electrical measurements confirmed that the presence of Mn induces a decrease in the electrical conductivity of the probed microstructures. Moreover, transition from direct tunneling to Fowler-Nordheim tunneling conduction mechanisms was found through the Mn-doped SnO_2 microplates. The analysis of the electrical measurements considering direct tunneling points out to an increase of the tunnel barrier through Mn doping. This tunnel barrier could be associated with the presence of surface states, the concentration of which is apparently enhanced by Mn doping. A modified direct tunneling mechanism involving two tunnel barriers at the front and rear surfaces of the probed structures has been also proposed. Based on the Poole-Frenkel mechanism, a value for the dielectric constant ε_r about 7.3 has been estimated for the SnO_2 microrods.

Acknowledgements

The work was[Q3] supported by MINECO/FEDER/M-ERA.Net. Cofund projects: MAT 2016-81720-REDC, MAT 2015-65274-R, and PCIN-2017-

106. MHZ thanks for the financial support by PAPIIT-UNAM IN101917 project.

Conflict of Interest

The[Q4] authors declare no conflict of interest.

Keywords

doping, EBIC, microplate, SnO_2

Received: April 5, 2018
Revised: May 14, 2018
Published online:

[1] X. M. Yin, C. C. Li, M. Zhang, Q. Hao, S. Liu, Q. H. Li, L. B. Chen, T. H. Wang, *Nanotechnology* **2009**, *20*, 455503.
[2] S. B. Sambhaji, A. T. Gauri, V. S. Arif, J. Oh-Shim, S. Myung-Mo, S. M. Rajaram, V. G. Anil, H. Sung-Hwan, *Mater. Lett.* **2012**, *79*, 29.
[3] G. Cannella, F. Principato, M. Foti, S. Di Marco, A. Grasso, S. Lombardo, *J. Appl. Phys.* **2011**, *110*, 024502.
[4] Z. Shu-Guo, Y. Shuang-Feng, W. Yu-Dan, L. Sheng-Lian, A. Chak-Tong, *Mater. Lett.* **2012**, *79*, 29.
[5] C. B. Fitzgerald, M. Venkatesan, L. S. Dorneles, R. Gunning, P. Stamenov, J. M. D. Coey, P. A. Stampe, R. J. Kennedy, E. C. Moreyra, U. S. Sias, *Phys. Rev. B* **2006**, *74*, 115307.
[6] J. Chi, H. Ge, J. Wang, Y. Zuo, L. Zhang, *J. Appl. Phys.* **2011**, *110*, 083907.
[7] S. Datta, B. Das, *Appl. Phys. Lett.* **1990**, *56*, 665.
[8] D. J. Monsma, J. C. Lodder, Th. J. A. Popma, B. Dieny, *Phys. Rev. Lett.* **1995**, *74*, 5260.
[9] M. Ishikawa, H. Sugiyama, T. Inokuchi, K. Hamaya, Y. Saito, *App. Phys. Lett.* **2012**, *100*, 252404.
[10] D. L. Smith, R. N. Silver, *Phys. Rev. B* **2001**, *64*, 045323.
[11] E. Kim, T. Yim, S. An, W.-J. Cho, K. Park, *Appl. Phys. Lett.* **2010**, *97*, 222107.
[12] J. D. Casperson, L. D. Bell, H. A. Atwater, *J. Appl. Phys.* **2002**, *92*, 261.
[13] M. Herrera, D. Maestre, A. Cremades, J. Piqueras, *J. Phys. Chem. C* **2013**, *117*, 8997.
[14] E. B. Yakimova, P. S. Vergelesa, A. V. Govorkovb, A. Y. Polyakovb, N. B. Smirnovb, L. In-Hwan, L. Cheul Ro, S. J. Pearton, *Superlatt. Microstruct.* **2009**, *45*, 308.
[15] A. Cremades, J. Piqueras, *J. Appl. Phys.* **1999**, *85*, 1438.
[16] J. Chen, T. Sekiguchi, D. Yang, F. Yin, K. Kido, S. Tsurekawa, *J. Appl. Phys.* **2004**, *96*, 5490.
[17] H. J. Leamy, *J. Appl. Phys.* **1962**, *53*, R51.
[18] S. Kim, T. Lim, S. Ju, *Nanotechnology* **2011**, *22*, 305704.
[19] D. Maestre, A. Cremades, J. Piqueras, *Semicond. Sci. Technol.* **2004**, *19*, 1236.
[20] R. Kumar-Chanana, *J. Appl. Phys.* **2011**, *109*, 104508.
[21] E. J. H. Lee, C. Ribeiro, T. R. Giraldi, E. Longo, E. R. Leite, J. A. Varela, *Appl. Phys. Lett.* **2004**, *84*, 1745.
[22] T. Ikuno, H. Okamoto, Y. Sugiyama, H. Nakato, F. Yamada, I. Kamiya, *Appl. Phys. Lett.* **2011**, *99*, 23107.
[23] M. Depas, B. Vermeire, P. W. Mertens, R. L. Van Meirhaeghe, M. M. Heyns, *Solid St. Electron.* **1995**, *38*, 1465.
[24] J. C. Ranuárez, M. J. Deen, C. H. Chen, *Microelectron. Reliab.* **2006**, *46*, 1939.
[25] T. Oh, *Trans. Electr. Electron. Mater.* **2017**, *18*, 21.
[26] M. Nagasawa, S. Shionoya, *Jpn. J. Appl. Phys.* **1971**, *10*, 727.
[27] M. Choueib, A. Ayari, P. Vicent, S. Perisanu, S. T. Purcell, *J. Appl. Phys.* **2011**, *109*, 73709.
[28] P. G. Li, X. Guo, X. F. Wang, W. H. Tang, *J. Alloys Compounds* **2009**, *479*, 74.
[29] M. Batzill, U. Diebold, *Prog. Surf. Sci.* **2005**, *79*, 47.

XXXX

M. Herrera, D. Maestre,*
A. Cremades

Surface Dielectric Tunnel Barrier Induced by Mn Doping in SnO_2 Micro- and Nanostructures

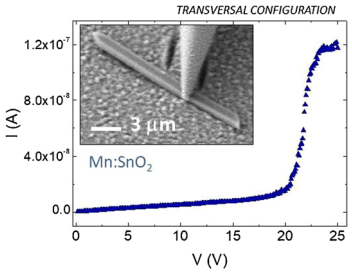

An electrically characterization of undoped and Mn doped SnO_2 microplates and rods, grown by a vapor–solid process, is performed. Mn doping induces a decrease in the electrical conductivity, as well as an increase of the surface dielectric tunnel barrier estimated from the analysis of the direct tunneling mechanism observed in the I–V curves.